Published in final edited form as:
*J Immunol*. 2012 August 15; 189(4): 1992–1999. doi:10.4049/jimmunol.1103207.

# GPR105 ablation prevents inflammation and improves insulin sensitivity in mice with diet-induced obesity

**Jianfeng Xu**[*], **Hidetaka Morinaga**[*], **Dayoung Oh**[*], **Pingping Li**[*], **Ai Chen**[*], **Saswata Talukdar**[*], **Eduardo Lazarowski**[‡], **Jerrold Olefsky**[*], and **Jane J. Kim**[†,§]

[*]Department of Medicine, University of California at San Diego, La Jolla, California, USA

[†]Department of Pediatrics, University of California at San Diego, La Jolla, California, USA

[‡]Department of Medicine, University of North Carolina, Chapel Hill, North Carolina, USA

[§]Rady Children's Hospital of San Diego, California, USA

## Abstract

GPR105, a G-protein coupled receptor for UDP-glucose, is highly expressed in several human tissues and participates in the innate immune response. Since inflammation has been implicated as a key initial trigger for type 2 diabetes, we hypothesized that GPR105 (official gene name: *P2RY14*) might play a role in the initiation of inflammation and insulin resistance in obesity. To this end, we investigated glucose metabolism in GPR105 knockout (KO) and wild-type (WT) mice fed a high-fat diet (HFD). We also examined whether GPR105 regulates macrophage recruitment to liver or adipose tissues by *in vivo* monocyte tracking and *in vitro* chemotaxis experiments, followed by transplantation of bone marrow from either KO or WT donors to WT recipients. Our data show that genetic deletion of GPR105 confers protection against HFD-induced insulin resistance, with reduced macrophage infiltration and inflammation in liver, and increased insulin-stimulated Akt phosphorylation in liver, muscle and adipose tissue. By tracking monocytes from either KO or WT donors, we found that fewer KO monocytes were recruited to the liver of WT recipients. Furthermore, we observed that UDP-Glc enhanced the *in vitro* migration of bone marrow-derived macrophages from WT but not KO mice, and that plasma UDP-Glc levels were significantly higher in obese versus lean mice. Finally, we confirmed that insulin sensitivity improved in HFD mice with a myeloid cell-specific deletion of GPR105. These studies indicate that GPR105 ablation mitigates HFD-induced insulin resistance by inhibiting macrophage recruitment and tissue inflammation. Hence, GPR105 provides a novel link between innate immunity and metabolism.

## INTRODUCTION

Insulin resistance is a major metabolic feature of obesity and a key factor in the pathogenesis of type 2 diabetes. Many lines of evidence show that the activation of proinflammatory pathways within insulin target tissues can impair insulin signaling, and chronic, low-level tissue inflammation is now recognized as an important cause of systemic insulin resistance (1). Several studies have shown that macrophages, a key component of the innate immune defense against pathogens, are critical effector cells in this proinflammatory process.

Macrophages present in non-inflamed tissues (resident macrophages) help maintain homeostasis and participate in tissue remodeling (2). However, in obese states, macrophages

Corresponding Author: Jane J. Kim, M.D., University of California, San Diego, 9500 Gilman Drive, MC 0673, La Jolla, CA 92093-0673, Tel: 858-534-8228, Fax: 858-534-6653, janekim@ucsd.edu.

accumulate in fat, liver and muscle tissues, secreting proinflammatory cytokines such as TNF-α and IL-6 that induce cellular insulin resistance by the activation of JNK or IκB kinase β signaling with serine phosphorylation of insulin receptor substrate proteins. Macrophages that are newly recruited following high-fat diet exposure have been shown to differ from resident macrophages in adipose tissue, showing increased proinflammatory properties (3). Although both innate and adaptive immune systems have been implicated in macrophage activation and recruitment in obesity (4), the precise mechanisms that regulate the recruitment of new macrophages to insulin target tissues are unclear.

G-protein coupled receptors (GPCRs) mediate a variety of physiological functions, which poise these proteins as therapeutic targets in metabolic disease. They are also the target of approximately half of all modern medicinal drugs (5). GPR105 (also known as the $P2Y_{14}$ receptor) is a member of a GPCR subgroup potently activated by pyrimidine UDP-sugars, especially uridine 5-diphosphoglucose (UDP-Glc) (6). GPR105 is broadly expressed in several human tissues, including the placenta, adipose tissue, stomach, intestine and discrete brain regions(6). Notably, GPR105 is also prominently expressed in immune cells, including macrophages, lymphocytes and neutrophils (7–9). Previous studies have revealed that GPR105 regulates leukocyte chemotaxis in response to UDP-Glc (10, 11).

Since, GPR105 participates in the innate immune response, we hypothesized that GPR105 may contribute to the initiation of obesity-induced insulin resistance. Here we have assessed the effects of whole body and bone marrow-specific deletion of GPR105 (official gene name: *P2ry14*) on insulin action and glucose homeostasis. We show that GPR105 in immune cells mediates macrophage recruitment to the liver in chronic HFD feeding with subsequent local inflammation and insulin resistance. Thus GPR105 may provide a novel link between innate immunity and insulin resistance.

## MATERIALS AND METHODS

### Animals

GPR105 (*P2ry14*) null mice were purchased from Taconic and have been previously described (12). Briefly, embryonic stem cells from 129P2 mice were manipulated by replacement of the *P2ry14* gene open reading frame by a *LacZ-neo* cassette and subsequently injected into C57BL/6J blastocytes to generate GPR105 KO mice. In our animal facility, these mice were back-crossed to C57Bl/6N mice obtained from Harlan Laboratories for 6 generations. Heterozygous mice from the $7^{th}$ generation were then used to breed WT and GPR105 KO littermates used for all experiments described here. Mice were fed either a normal chow (NC) or HFD (60% kcal from fat; D12492, Research Diets), and maintained on a 12h light/dark cycle with free access to food and water. For bone marrow transplantation studies, 10w C57BL/6N mice (Harlan, California) were exposed to 10-Gy of Co-60 irradiation and injected with bone marrow cells from WT or GPR105 KO mice within 24h. Eight weeks after transplantation, mice were fed either NC or HFD for 12w to generate lean or obese/insulin resistant phenotypes. All mouse procedures conformed to the Guide for Care and Use of Laboratory Animals of the US National Institutes of Health and were approved by the Animal Subjects Committee of the University of California, San Diego.

### Metabolic studies

Glucose and insulin tolerance tests (GTT and ITT, respectively) were performed on 7h fasted mice. Animals were given intraperitoneal or oral dextrose (1 g/kg, Hospira, Inc.) for the GTT, or intraperitoneal insulin (0.6 U/kg, Novolin R, Novo-Nordisk) for the ITT. Glucose levels after injection were monitored over time. Blood samples were drawn by tail nick at basal and indicated times, and glucose was measured using a One-Touch glucose

meter (Lifescan). Hyperinsulinemic-euglycemic clamp studies were performed as previously described (13, 14). In brief, two jugular catheters were inserted under anesthesia, tunneled to the mid-scapular region and externalized. Five days later, the clamp experiments began with the infusion of an equilibration solution of D-[3-$^3$H] glucose (NEN, Boston) for 90 min at a constant rate of 5 μCi/h. Then, insulin was infused at 8 mU/kg/min while the glucose infusion rate was adjusted as necessary until euglycemia was achieved (~120 mg/dl for >20 min). Blood samples were collected prior to insulin infusion and upon euglycemia to confirm steady-state. At steady-state, the rate of glucose disappearance (total glucose disposal rate or GDR) equals the sum of hepatic glucose production (HGP) and the glucose infusion rate (GIR). The insulin-stimulated GDR (IS-GDR) is equal to the total GDR minus the basal glucose turnover rate. Serum insulin levels were analyzed by ELISA (Alpco Diagnostics).

### Triglyceride and glycogen measurements

Triglyceride (TG) content was measured in liver homogenates in PBS containing 5% Triton X-100 and in plasma samples (EnzyChrom™, BioAssay Systems, Hayward, CA). Glycogen levels were measured by the method of Seifter et al. (15).

### Histology

H&E staining in liver and adipose tissue sections was conducted by the University of California, San Diego histology core at the Moore's Cancer Center. Anti-Mac2 (Cedarlane Labs) and Anti-F4/80 (Abcam, MA) antibodies were used for immunohistochemistry.

### Immunoblot analysis

For insulin-stimulated phospho-Akt analysis, mice were fasted for 7h and then injected with 0.2 U/kg insulin via the inferior vena cava under anesthesia. Tissues were taken before or after injection (3 min for liver and 10 min for epididymal white adipose tissue [eWAT] and skeletal muscle), snap frozen, and subjected to western blot analyses performed according to standard techniques. Antibodies against p-Akt (Ser473), Akt and α-tubulin were obtained from Cell Signaling Technologies (Beverly, MA). To measure Akt phosphorylation, solubilized extracts containing equal amounts of tissue protein were immunoblotted with rabbit polyclonal antibodies against either Akt or phospho-Ser473 Akt (Cell Signaling Technology, Beverly, MA), followed by second antibody detection. For quantification, the relative intensities of protein bands were measured with ImageJ and expressed as arbitrary units.

### RNA isolation and quantitative RT-PCR

Total RNA was isolated from cells and tissues using TRIzol Reagent (Invitrogen, Carlsbad, CA) according to the manufacturer's instructions. First strand cDNA was synthesized using a High-Capacity cDNA Reverse Transcription Kit (Applied Biosystems, Foster City, CA). The samples were run in 20 μl reactions using an MJ Research PTC-200 96 well thermocycler coupled with the Chromo 4 Four-Color Real-Time System (GMI, Inc., Ramsey, MN). Gene expression levels were calculated after normalization to the standard housekeeping gene *RNA polymerase II (RPII)* using the $\Delta\Delta C_T$ method as described previously (16). Primer sequences are available in supplemental Table S1.

### Monocyte tracking

Blood collected from the retro-orbital sinus of WT or GPR105 KO mice was subjected to red blood cell lysis, and monocyte subsets were enriched with the EasySep® mouse monocytes enrichment kit (STEMCELL Technologies, Vancouver, BC). Isolated monocytes from 10–15 mice of each genotype were pooled together. These monocytes ($5\times10^5$ to

$10\times10^5$) were then washed in serum-free RPMI and suspended in 2 ml of Diluent solution C. PKH26 (Sigma-Aldrich, St Louis, MO) dissolved at $2\times10^{-3}$ M in Diluent C was added, and the cells were incubated for 10 min at room temperature in the dark. The staining reaction was halted by the addition of an equal volume of medium supplemented with 10% FBS. The mixture was centrifuged, and the cells were washed once and re-suspended in serum-containing medium. Subsequent to labeling with PKH26, the monocytes were counted and ~$1\times10^5$ viable cells were suspended in 0.2 ml PBS and injected into the femoral vein of WT mice who were receiving HFD. Five days after injection, adipose tissue macrophages (ATMs) and liver non-parenchymal cells were isolated and analyzed by FACS analysis.

### FACS analysis of macrophages from the adipose stromal vascular fraction and liver

Epididymal fat pads were weighed, rinsed in PBS, and then minced in FACS buffer (PBS/1% BSA). Adipocytes and stromal vascular cells were prepared from collagenase-digested adipose tissue (17). Liver macrophage cells were prepared by a two-step liver collagenase digestion and fractionation on a density gradient (18). FACS analysis of stromal vascular cells for macrophage content and subtypes were performed as previously described (17). The antibodies used for surface staining were F4/80 (BM8), CD11b (M1/70) and CD11c (N418) (eBioscience, San Diego, CA).

### BMDM culture and *in vitro* chemotaxis assay

Bone marrow-derived macrophage (BMDM) culture was performed as previously described (17). Briefly, bone marrow cells were flushed from the femurs and tibias of 10–12-week-old WT and GPR105 KO mice. The cells were then differentiated into BMDMs in RPMI medium containing recombinant M-CSF, low endotoxin FBS and streptomycin/penicillin. Five days after differentiation, cells were harvested and suspended in DMEM with 1g/L glucose. The *in vitro* chemotaxis assay was performed as previously described (19). Approximately $10^5$ cells were seeded into the upper chamber of an 8 μM polycarbonate filter (24-transwell format; Corning, Lowell, MA), and DMEM with indicated concentrations of UDP-Glc was placed in the lower chamber. After 3h, the cells that had migrated to the lower chamber were counted.

### Measurement of UDP-glucose levels in plasma

Plasma samples were deproteinized with 5% trichloroacetic acid (TCA) followed by ethyl ether extraction and neutralization. The UDP-Glc content in the extracts was quantified using the assay that is based on enzymatic conversion of 32P-pyrophosphate (32PPi) + UDP-glucose into [32P]UTP + glucose-1P, as previously described(20). Briefly, samples were incubated for 1 h in the presence of 1 U/ml UDP-Glc pyrophosphorylase from baker's yeast (Sigma) and 100 nM 0.1 μCi 32-PPi (Perkin Elmer). Incubations were terminated by the addition of 0.5 mM PPi and subsequent heating (2 min at 95°C). The resulting 32P-species were separated by HPLC, via a Nova-Pack C18 column (Waters), and quantified on-line with a Flo-One 500TR Radiomatic analyzer (Packard). A calibration curve using known amounts of UDP-glucose (Fluka) was performed in parallel.

### Statistical Analysis

All values are expressed as means ± SEM unless otherwise noted. We used Student's two-tailed t-test or ANOVA to determine differences between groups, and repeated measures ANOVA testing for comparisons over time. $P$ values of $<0.05$ were considered significant.

# RESULTS

## GPR105 deletion protects mice from high fat diet-induced insulin resistance

To investigate the functional role of GPR105 in HFD-induced obesity, 8-week-old GPR105 KO and their wild-type littermates were fed a NC or 60% HFD for 16 weeks. Whole body weights did not differ between GPR105 KO mice and their WT controls on either diet (Figure 1A). HFD food intake was also similar between genotypes (Figure 1B).

On the NC diet, there were no differences in glucose tolerance (Figure 1C) or fasting insulin levels (Figure 1D) between WT and GPR105 KO mice. Following HFD-feeding, WT mice developed severe glucose intolerance, as expected (Figure 1C). However, HFD-fed GPR105 KO mice were protected from HFD-induced defects in glucose tolerance, with significantly lower glucose excursions during the IPGTT (Figure 1C). Despite similar basal glucose values, fasting insulin levels were also lower in HFD GPR105 KO mice compared to WT controls (Figure 1D and E), suggesting that the improved glucose tolerance was secondary to reduced insulin resistance. This finding was further supported by decreased insulin values measured 15 min following an oral dextrose challenge (Figure 1E) and a greater hypoglycemic response during ITT (Figure 1F) in HFD-fed GPR105 KO mice. These data indicate improved insulin sensitivity in HFD-fed obese GPR105 KO mice.

## Improved insulin sensitivity in HFD-fed GPR105 KO mice

To further investigate *in vivo* insulin sensitivity in HFD-fed WT and GPR105 KO mice, we performed hyperinsulinemic-euglycemic glucose clamp studies. These studies further supported our GTT and ITT findings with a 3-fold increase in the glucose infusion rate in GPR105 KO mice compared to controls (Figure 2A). Total glucose turnover (Figure 2B) and insulin-stimulated glucose disposal rates (IS-GDR) (Figure 2C) were also significantly enhanced in GPR105 KO mice. Since 70–80% of the IS-GDR is attributable to skeletal muscle glucose uptake, these results suggest that the deletion of GPR105 leads to improved skeletal muscle insulin sensitivity.

GPR105 KO mice also demonstrated significantly lower rates of hepatic glucose production (HGP) under both basal and steady-state clamp conditions (Figure 2D), indicating that the ability of insulin to suppress HGP was enhanced in HFD-fed GPR105 KO mice (Figure 2E). Consistent with the improved hepatic and skeletal muscle insulin sensitivity found in the clamp studies, AKT phosphorylation was significantly increased in liver, adipose and skeletal muscle tissues of GPR105 KO mice following insulin stimulation (Figure 2F). Taken together, these *in vivo* results support the conclusion that GPR105 KO mice exhibit improved systemic insulin sensitivity following HFD with enhanced insulin action in liver, skeletal muscle and adipose tissues.

## Reduced liver steatosis and inflammation in GPR105 KO mice

Liver weights were decreased in the GPR105 KO mice (Figure 3A) despite the similar body weights of GPR105 KO and WT mice. GPR105 KO mice also demonstrated lower liver triglyceride and glycogen content (Figure 3B and C) as well as a lower grade of hepatic steatosis by histology (Figure 3D).

Notably, although GPR105 KO mice exhibited improved hepatic insulin sensitivity, GPR105 expression was much lower in hepatocytes compared to non-parenchymal cells which include Kupffer cells, recruited macrophages, and other immune cell types (Figure 3E). Therefore, we considered that the improved metabolic phenotype in the liver could be attributable to crosstalk between hepatocytes and these immune cell types. Interestingly, immunohistochemistry with F4/80, a marker of tissue macrophages (21), showed reduced

F4/80 staining in liver from HFD-fed GPR105 KO mice when compared to WT controls, suggesting a reduced number of either Kupffer cells or recruited macrophages in the absence of GPR105 (Figure 3F).

Flow cytometry analysis of non-parenchymal cells from HFD liver showed a significantly lower percentage of F4/80+ cells from GPR105 KO mice (Figure 3G), consistent with reduced liver inflammation. Furthermore, gene expression of several pro-inflammatory cytokines (IL-1β, IL-10, IL-6 and TNF-α) was profoundly diminished in liver tissues from GPR105 KO mice (Figure 3H). Of note, fatty acid synthetase (FAS) and ACC were decreased, while peroxisomal proliferator-activated receptor (PPAR)α, medium-chain acyl-CoA dehydrogenase (MCAD), PPARγ coactivator-1 (PGC1)β, mitochondrial transcription factor A (TFAM), and subunit 2 of cytochrome *c* oxidase (COX2) were increased (Figure 4G), suggesting that decreased lipogenesis and increased fatty acid oxidation may both contribute to the improved hepatic steatosis observed in GPR105 KO mice.

## Adipose tissue characteristics of GPR105 KO mice

HFD-induced adipose tissue inflammation is an important initial event in the development of insulin resistance, occurring as early as 3d following the initiation of HFD (22). Therefore, we examined adipose tissue from HFD-fed GPR105 KO and WT mice. No significant differences in eWAT weights were observed between genotypes (Figure 4A). Interestingly, GPR105 expression was detected only at low levels in adipocytes but was highly expressed in the stromal vascular fraction (Figure 4B), similar to the liver where GPR105 was only marginally expressed in hepatocytes, but highly expressed in the non-parenchymal cells.

ATMs increase in obesity (17, 23), and a specific subpopulation of $CD11c^+$, M1-like macrophages has been shown to secrete pro-inflammatory cytokines that reduce insulin sensitivity (17, 24). Although liver macrophages were reduced in number, immunohistochemistry staining of epididymal adipose tissue with the macrophage marker Mac2 did not show significant differences in crown-like structures in fat tissue (Figure 4C). Likewise, flow cytometry did not show differences in either F4/80+CD11b+ (double positive) macrophages (Figure 4D) or F4/80+CD11b+CD11c+ (triple positive) macrophages (Figure 4E) in the eWAT stromal vascular fraction from GPR105 KO mice. We were also unable to detect significant changes in pro-inflammatory gene expression. Although IL-1β gene expression decreased, similar changes were not observed in TNFα and IL-6 gene expression (Figure 4F).

## GPR105 deletion reduces macrophage chemotaxis *in vivo* and *in vitro*

Since GPR105 depletion resulted in reduced macrophage numbers in liver, we next investigated whether this phenomenon could be attributed to decreased macrophage recruitment versus increased macrophage turnover. We therefore conducted an *in vivo* monocyte tracking experiment to assess the ability of WT or GPR105 null monocytes to migrate into liver and adipose tissues. We verified that the monocytes comprised over 90% of WBC population after enrichment (Figure S1). PKH26-labeled monocytes isolated from either GPR105 KO or WT donor mice were injected intravenously to WT recipient mice on HFD. Five days after injection, PKH26-labeled cells in the non-parenchymal cell fraction were counted by flow cytometry. We have previously shown that macrophages represent >90% of the PKH-labeled cells recruited to the non-parenchymal fraction of both liver and adipose tissue (25).

As shown in Figure 5A, fewer liver PKH26+ monocytes were identified in mice that received GPR105 KO monocytes (Figure 5A). In contrast, the percentage of PKH26+ cells

in the adipose stromal vascular fraction did not differ between the two groups (Figure 5B). These results indicate that GPR105 plays a role in monocyte responsiveness to chemoattract signals from liver, but not from adipose tissue. Moreover, the magnitude of decrease in liver PKH26+ cells in GPR105 KO mice suggest that the decrease in liver F4/80+ cells (Figure 3G) likely reflects a difference in macrophage recruitment rather than resident tissue macrophages (Kupffer cells) in HFD-fed GPR105 KO mice.

UDP-Glc acts as a potent endogenous agonist for GPR105 and is a substrate for glycogen synthetase and protein glycosylation. Therefore we explored the potential role of UDP-Glc as a chemoattractant released from liver tissues following HFD. To test whether UDP-Glc could induce chemotaxis in a GPR105-mediated manner, we performed an *in vitro* chemotaxis assay to determine whether increasing concentrations of UDP-Glc would induce the migration of bone marrow derived macrophages derived from WT or GPR105 KO donor mice. As shown in Figure 5C and D, we observed that 1mM UDP-Glc produced a 2.5-fold increase in the migration of BMDMs from WT mice whereas this effect was abolished for BMDMs from GPR105 KO mice.

Since UDP-Glc potentially represents an extracellular signaling molecule that could promote the recruitment of macrophages in obese states, we next measured UDP-Glc levels in plasma collected from mice fed either normal chow or HFD in order to determine whether UDP-Glc levels increase in obesity. By employing HPLC analysis of nucleotide sugars, we discovered that plasma UDP-Glc levels are significantly higher in obese mice (16.66 ± 3.42 nM in HFD-fed vs. 4.70 ± 1.29 nM in standard chow-fed mice, $p<0.005$) (Figure 5E).

### Improved insulin sensitivity following transplantation of GPR105-depleted bone marrow

To further investigate whether differences in macrophage recruitment could account for the difference in insulin resistance phenotypes between whole-body GPR105 KO and WT mice, we performed bone marrow transplantation (BMT) studies by injecting bone marrow cells from either GPR105 KO (KO-BMT) or WT (WT-BMT) donors into irradiated WT recipients. After reconstitution, GPR105 expression was barely detectable in circulating white blood cells from KO BMT mice, showing nearly complete replacement of the bone marrow with donor cells after transplant (Figure S2). We observed that KO-BMT mice demonstrated a similar phenotype to the whole body knockout. As shown in Figure 6A, glucose tolerance was similar between NC-fed KO-BMT and WT-BMT mice. However, following a 12w HFD, KO-BMT mice exhibited a significant improvement in glucose tolerance compared to diet-matched WT-BMT controls (Figure 6A).

This protection from HFD-induced insulin resistance in KO-BMT mice was further supported by hyperinsulinemic-euglycemic clamp studies which showed that the glucose infusion rate and insulin-stimulated glucose disposal rate were significantly higher in KO-BMT mice than WT-BMT mice (Figure 6B and C). Insulin-stimulated suppression of hepatic glucose output was somewhat enhanced in KO-BMT mice, although this difference did not reach statistical significance (Figure 6D). Consistent with improved insulin sensitivity, we found that insulin-stimulated AKT phosphorylation significantly increased in liver, adipose and skeletal muscle of KO-BMT mice (Figure 6E).

## DISCUSSION

Chronic tissue inflammation is now recognized as a key cause of systemic insulin resistance in the context of obesity and Type 2 diabetes. A substantive literature has emerged indicating that the accumulation of activated macrophages in tissues provides a mechanism for inflammation-induced insulin resistance, since these cells secrete a variety of cytokines which can directly impair insulin sensitivity in insulin target cells. Other immune cell types

such as lymphocytes and eosinophils can also participate in these events, but their effects are likely mediated by modulating macrophage chemotaxis and activation. Thus, the macrophage would be the effector cell, causing decreased insulin sensitivity. Here, we report the role of a macrophage-expressed GPCR termed GPR105, which, heretofore, has not been implicated in obesity-associated chronic tissue inflammation and insulin resistance.

GPR105 (also known as the $P2Y_{14}$ receptor) is a member of the P2Y purinergic receptor subfamily. P2Y receptor subtypes have been identified in immune cells such as monocytes and macrophages and exert effects on inflammatory signaling (26). For example, $P2Y_2$ receptors regulate macrophage chemotaxis toward complement C5a in response to ATP release via autocrine purinergic signaling (26). Unlike other P2Y receptors that are activated by adenine and/or uracil nucleotides, GPR105 is a membrane receptor for UDP-glucose.

GPR105 expression has been reported in various human tissues, including the placenta, adipose tissue, spleen, gut and discrete brain regions by microarray or quantitative PCR (6, 7). However, since immune cells are widely distributed among several tissue types, it was previously unknown whether GPR105 is expressed by parenchymal or non-parenchymal cells.

In this report, we demonstrate that GPR105 is highly expressed in the stromal vascular fraction but not in the parenchymal fraction of liver and adipose tissue. Therefore, the tissue-specific role of GPR105 requires careful interpretation since crosstalk between resident immune and parenchymal cells within tissues and crosstalk with circulating leukocytes may account for the *in vivo* phenotypes.

We show that GPR105 knockout mice are more insulin sensitive with reduced liver steatosis and inflammation following HFD feeding. In addition, GPR105 mediates macrophage chemotaxis to UDP-Glc *in vitro* and macrophage recruitment to liver tissues in response to HFD *in vivo*. Notably, the most impressive phenotypic changes in HFD GPR105 KO mice were observed in the liver. Hepatic insulin resistance in obesity is associated with increased expression of inflammatory mediators and massive accumulation of intracellular lipid within hepatocytes. Recruited hepatic macrophages (RHMs) and resident Kupffer cells are important immune cell types in the liver and reside in the sinusoids where they are poised to communicate with hepatocytes. Improved hepatic insulin sensitivity in HFD GPR105 KO mice was associated with decreased recruited macrophage numbers, reduced tissue inflammation, and reduced hepatic steatosis. Our monocyte tracking studies corroborated these data, showing reduced migration of macrophages to the liver in HFD mice.

We also demonstrated that macrophage chemotaxis was mediated by GPR105 as BMDMs obtained from GPR105 KO mice displayed significantly impaired migration towards a UDP-Glc gradient in an *in vitro* transwell assay. GPR105 has been previously implicated in the migration of immune cells. For example, GPR105 expressed in primitive hematopoietic cells regulates the chemotaxis of these cells to conditioned media from the bone marrow stroma (10). GPR105 expressed in endometrial tissues of the female reproductive tract also facilitates the chemotaxis of neutrophils in response to UPDG (11). In our study, we observed that fewer monocytes from GPR105 KO mice were recruited to the liver in response to HFD *in vivo*.

Interestingly, increased hepatic UDP-Glc has been reported in association with the development of obesity (27, 28). UDP-Glc has been shown to be a functional agonist for GPR105 mediated cellular responses in various cell types (29–34), and the endoplasmic reticulum and golgi apparatus provides the major route for extracellular release of UDP-Glc (35). Furthermore, damaged cells may release nucleotides such as ATP and UDP-Glc during inflammation and mechanical stress (11). Since HFD-induced lipotoxicity and inflammation

have been shown to increase hepatocellular apoptosis and necrosis (36–38), we hypothesize that UDP-Glc may act as an extracellular signaling molecule and chemoattractant for macrophage recruitment via GPR105. In this study, we were able to demonstrate for the first time that UDP-Glc levels in plasma are significantly higher in obese compared to lean mice. Although further investigation is required to address this hypothesis, our results suggest that UDP-Glc release from hepatocellular injury may trigger innate immune responses and promote the development of hepatic insulin resistance.

In addition to improved hepatic insulin sensitivity, we observed improved global insulin sensitivity in whole-body GPR105 KO mice, with enhanced insulin action not only in liver, but also in skeletal muscle and adipose tissue. GPR105 is expressed at only very low levels in murine muscle (7). Furthermore, we were unable to detect significant changes in proinflammatory gene expression in adipose tissue. Prior studies have shown that strategies that exclusively target insulin action in the liver can alter insulin sensitivity in extrahepatic tissues (39, 40) by modifying circulating glucose. Thus, the improved insulin sensitivity in muscle and fat of GPR105 KO mice could be secondary to indirect effects from the liver. However, myeloid cells have been shown to be responsible for cross-talk involving proinflammatory cytokines between insulin-responsive tissues (41). Since we observed significantly improved insulin sensitivity in mice with a myeloid-specific GPR105 deletion obtained by bone marrow transplantation, myeloid cells appear to play a primary role in GPR105-mediated inflammation and insulin resistance in our study as well. Bone marrow transplantation results in the reconstitution of several immune cell types in addition to macrophages. Therefore, we cannot conclude that GPR105 in lymphocytes or other immune cells does not contribute to our observed phenotype.

We have recently shown that recruited hepatic macrophages comprise over half of the population of liver macrophages under HFD conditions (25). These cells are radio-sensitive and turn over in a matter of weeks so that the RHMs in the KO BMT mice are essentially donor-derived. On the other hand, the majority of resident Kupffer cells are radio-resistant and turn over more slowly (42, 43) so they are probably not fully replaced at the time of our studies (20 weeks after BMT). In contrast, the nearly all of the adipose tissue macrophages are donor-derived after 8 weeks reconstitution and 12 weeks high fat feeding (Figure S3). To the extent that chimerism of the Kupffer cells population exists at the time of our studies, this would tend to underestimate the effect of GPR105 ablation on the hepatic phenotype, consistent with the results of our clamp studies showing a smaller improvement in hepatic glucose suppression in the KO BMT mice than that observed in the whole body GPR105 knockouts. Thus, our data overall suggest that GPR105-mediated macrophage recruitment to the liver following HFD propagates strong inflammatory signals in the liver that may enter the circulation to cause peripheral insulin resistance in other tissues such as muscle and fat.

In this study, we have expanded our understanding of GPR105 *in vivo* by demonstrating that GPR105 null mice are protected from HFD-induced insulin resistance. This improvement in systemic insulin sensitivity was accompanied by decreased macrophage infiltration and a reduction in inflammation in the liver. We also showed that GPR105 mediates monocyte migration to the liver in response to HFD, and that myeloid-specific deletion of GPR105 results in improved insulin sensitivity. Taken together, these data support the conclusion that GPR105 participates in macrophage recruitment to the liver in chronic HFD feeding with subsequent local inflammation and insulin resistance. Novel therapeutic strategies that inhibit GPR105 and prevent macrophage migration may prove to be protective to the development of insulin resistance and type 2 diabetes.

## Supplementary Material

Refer to Web version on PubMed Central for supplementary material.

## Acknowledgments

We thank Merck Pharmaceuticals for providing GPR105 KO mice as well as additional research support for this project.

This work was supported by National Institute of Health grants DK075479 (to JJK) and DK033651, DK074868, T32 DK 007494, DK 090962 and DK063491 (to JMO). This work was also supported by the Eunice Kennedy Shriver NICHD/NIH through cooperative agreement of U54 HD 012303-25 as part of the specialized Cooperative Centers Program in Reproduction and Infertility Research.

## References

1. Olefsky JM, Glass CK. Macrophages, Inflammation, and Insulin Resistance. Annual Review of Physiology. 2010; 72:219–246.
2. Gordon S, Taylor PR. Monocyte and macrophage heterogeneity. Nat Rev Immunol. 2005; 5:953–964. [PubMed: 16322748]
3. Lumeng CN, Deyoung SM, Bodzin JL, Saltiel AR. Increased inflammatory properties of adipose tissue macrophages recruited during diet-induced obesity. Diabetes. 2007; 56:16–23. [PubMed: 17192460]
4. Thewissen MM, Damoiseaux JG, Duijvestijn AM, van Greevenbroek MM, van der Kallen CJ, Feskens EJ, Blaak EE, Schalkwijk CG, Stehouwer CD, Cohen Tervaert JW, Ferreira I. Abdominal fat mass is associated with adaptive immune activation: the CODAM Study. Obesity (Silver Spring). 2011; 19:1690–1698. [PubMed: 21253003]
5. Filmore, D. Modern Drug Discovery. American Chemical Society; 2004. It's a GPCR world; p. 24-28.
6. Chambers JK, Macdonald LE, Sarau HM, Ames RS, Freeman K, Foley JJ, Zhu Y, McLaughlin MM, Murdock P, McMillan L, Trill J, Swift A, Aiyar N, Taylor P, Vawter L, Naheed S, Szekeres P, Hervieu G, Scott C, Watson JM, Murphy AJ, Duzic E, Klein C, Bergsma DJ, Wilson S, Livi GP. A G protein-coupled receptor for UDP-glucose. J Biol Chem. 2000; 275:10767–10771. [PubMed: 10753868]
7. Freeman K, Tsui P, Moore D, Emson PC, Vawter L, Naheed S, Lane P, Bawagan H, Herrity N, Murphy K, Sarau HM, Ames RS, Wilson S, Livi GP, Chambers JK. Cloning, pharmacology, and tissue distribution of G-protein-coupled receptor GPR105 (KIAA0001) rodent orthologs. Genomics. 2001; 78:124–128. [PubMed: 11735218]
8. Moore DJ, Murdock PR, Watson JM, Faull RL, Waldvogel HJ, Szekeres PG, Wilson S, Freeman KB, Emson PC. GPR105, a novel Gi/o-coupled UDP-glucose receptor expressed on brain glia and peripheral immune cells, is regulated by immunologic challenge: possible role in neuroimmune function. Brain Res Mol Brain Res. 2003; 118:10–23. [PubMed: 14559350]
9. Lattin JE, Schroder K, Su AI, Walker JR, Zhang J, Wiltshire T, Saijo K, Glass CK, Hume DA, Kellie S, Sweet MJ. Expression analysis of G Protein-Coupled Receptors in mouse macrophages. Immunome Res. 2008; 4:5. [PubMed: 18442421]
10. Lee BC, Cheng T, Adams GB, Attar EC, Miura N, Lee SB, Saito Y, Olszak I, Dombkowski D, Olson DP, Hancock J, Choi PS, Haber DA, Luster AD, Scadden DT. P2Y-like receptor, GPR105 (P2Y14), identifies and mediates chemotaxis of bone-marrow hematopoietic stem cells. Genes Dev. 2003; 17:1592–1604. [PubMed: 12842911]
11. Arase T, Uchida H, Kajitani T, Ono M, Tamaki K, Oda H, Nishikawa S, Kagami M, Nagashima T, Masuda H, Asada H, Yoshimura Y, Maruyama T. The UDP-Glucose Receptor P2RY14 Triggers Innate Mucosal Immunity in the Female Reproductive Tract by Inducing IL-8. The Journal of Immunology. 2009; 182:7074–7084. [PubMed: 19454705]
12. Bassil AK, Bourdu S, Townson KA, Wheeldon A, Jarvie EM, Zebda N, Abuin A, Grau E, Livi GP, Punter L, Latcham J, Grimes AM, Hurp DP, Downham KM, Sanger GJ, Winchester WJ, Morrison AD, Moore GB. UDP-glucose modulates gastric function through P2Y14 receptor-dependent and -

independent mechanisms. Am J Physiol Gastrointest Liver Physiol. 2009; 296:G923–930. [PubMed: 19164486]

13. Oh DY, Talukdar S, Bae EJ, Imamura T, Morinaga H, Fan W, Li P, Lu WJ, Watkins SM, Olefsky JM. GPR120 Is an Omega-3 Fatty Acid Receptor Mediating Potent Anti-inflammatory and Insulin-Sensitizing Effects. Cell. 2010; 142:687–698. [PubMed: 20813258]
14. Lu M, Sarruf DA, Talukdar S, Sharma S, Li P, Bandyopadhyay G, Nalbandian S, Fan W, Gayen JR, Mahata SK, Webster NJ, Schwartz MW, Olefsky JM. Brain PPAR-[gamma] promotes obesity and is required for the insulin-sensitizing effect of thiazolidinediones. Nat Med. 2011; 17:618–622. [PubMed: 21532596]
15. Seifter S, Dayton S, et al. The estimation of glycogen with the anthrone reagent. Arch Biochem. 1950; 25:191–200. [PubMed: 15401229]
16. Yoshizaki T, Milne JC, Imamura T, Schenk S, Sonoda N, Babendure JL, Lu JC, Smith JJ, Jirousek MR, Olefsky JM. SIRT1 Exerts Anti-Inflammatory Effects and Improves Insulin Sensitivity in Adipocytes. Mol Cell Biol. 2009; 29:1363–1374. [PubMed: 19103747]
17. Nguyen MT, Favelyukis S, Nguyen AK, Reichart D, Scott PA, Jenn A, Liu-Bryan R, Glass CK, Neels JG, Olefsky JM. A subpopulation of macrophages infiltrates hypertrophic adipose tissue and is activated by free fatty acids via Toll-like receptors 2 and 4 and JNK-dependent pathways. J Biol Chem. 2007; 282:35279–35292. [PubMed: 17916553]
18. Nnalue NA, Shnyra A, Hultenby K, Lindberg AA. Salmonella choleraesuis and Salmonella typhimurium associated with liver cells after intravenous inoculation of rats are localized mainly in Kupffer cells and multiply intracellularly. Infect Immun. 1992; 60:2758–2768. [PubMed: 1612743]
19. Patsouris D, Neels JG, Fan W, Li PP, Nguyen MTA, Olefsky JM. Glucocorticoids and Thiazolidinediones Interfere with Adipocyte-mediated Macrophage Chemotaxis and Recruitment. J Biol Chem. 2009; 284:31223–31235. [PubMed: 19740750]
20. Lazarowski ER, Shea DA, Boucher RC, Harden TK. Release of cellular UDP-glucose as a potential extracellular signaling molecule. Mol Pharmacol. 2003; 63:1190–1197. [PubMed: 12695547]
21. Austyn JM, Gordon S. F4/80, a monoclonal antibody directed specifically against the mouse macrophage. European Journal of Immunology. 1981; 11:805–815. [PubMed: 7308288]
22. Lee YS, Li P, Huh JY, Hwang IJ, Lu M, Kim JI, Ham M, Talukdar S, Chen A, Lu WJ, Bandyopadhyay GK, Schwendener R, Olefsky J, Kim JB. Inflammation Is Necessary for Long-Term but Not Short-Term High-Fat Diet induced Insulin Resistance. Diabetes. 2011; 60:2474–2483. [PubMed: 21911747]
23. Xu H, Barnes GT, Yang Q, Tan G, Yang D, Chou CJ, Sole J, Nichols A, Ross JS, Tartaglia LA, Chen H. Chronic inflammation in fat plays a crucial role in the development of obesity-related insulin resistance. J Clin Invest. 2003; 112:1821–1830. [PubMed: 14679177]
24. Lumeng CN, Bodzin JL, Saltiel AR. Obesity induces a phenotypic switch in adipose tissue macrophage polarization. J Clin Invest. 2007; 117:175–184. [PubMed: 17200717]
25. Oh DY, Morinaga H, Talukdar S, Bae EJ, Olefsky JM. Increased macrophage migration into adipose tissue in obese mice. Diabetes. 2012; 61:346–354. [PubMed: 22190646]
26. Ferrero ME. Purinoceptors in inflammation: potential as anti-inflammatory therapeutic targets. Front Biosci. 2011; 17:2172–2186. [PubMed: 21622169]
27. van de Werve G. Fasting enhances glycogen synthase activation in hepatocytes from insulin-resistant genetically obese (fa/fa) rats. Biochem J. 1990; 269:789–794. [PubMed: 1697164]
28. Veerababu G, Tang J, Hoffman RT, Daniels MC, Hebert LF Jr, Crook ED, Cooksey RC, McClain DA. Overexpression of glutamine: fructose-6-phosphate amidotransferase in the liver of transgenic mice results in enhanced glycogen storage, hyperlipidemia, obesity, and impaired glucose tolerance. Diabetes. 2000; 49:2070–2078. [PubMed: 11118009]
29. Skelton L, Cooper M, Murphy M, Platt A. Human immature monocyte-derived dendritic cells express the G protein-coupled receptor GPR105 (KIAA0001, P2Y14) and increase intracellular calcium in response to its agonist, uridine diphosphoglucose. J Immunol. 2003; 171:1941–1949. [PubMed: 12902497]

30. Scrivens M, Dickenson JM. Functional expression of the P2Y14 receptor in murine T-lymphocytes. Br J Pharmacol. 2005; 146:435–444. [PubMed: 15997228]

31. Scrivens M, Dickenson JM. Functional expression of the P2Y14 receptor in human neutrophils. Eur J Pharmacol. 2006; 543:166–173. [PubMed: 16820147]

32. Krzeminski P, Pomorski P, Baranska J. The P2Y14 receptor activity in glioma C6 cells. Eur J Pharmacol. 2008; 594:49–54. [PubMed: 18638471]

33. Dovlatova N, Wijeyeratne YD, Fox SC, Manolopoulos P, Johnson AJ, White AE, Latif ML, Ralevic V, Heptinstall S. Detection of P2Y(14) protein in platelets and investigation of the role of P2Y(14) in platelet function in comparison with the EP(3) receptor. Thromb Haemost. 2008; 100:261–270. [PubMed: 18690346]

34. Gao ZG, Ding Y, Jacobson KA. UDP-glucose acting at P2Y14 receptors is a mediator of mast cell degranulation. Biochem Pharmacol. 2010; 79:873–879. [PubMed: 19896471]

35. Sesma JI, Esther CR, Kreda SM, Jones L, O'Neal W, Nishihara S, Nicholas RA, Lazarowski ER. Endoplasmic Reticulum/Golgi Nucleotide Sugar Transporters Contribute to the Cellular Release of UDP-sugar Signaling Molecules. Journal of Biological Chemistry. 2009; 284:12572–12583. [PubMed: 19276090]

36. Wang Y, Ausman LM, Russell RM, Greenberg AS, Wang XD. Increased apoptosis in high-fat diet-induced nonalcoholic steatohepatitis in rats is associated with c-Jun NH2-terminal kinase activation and elevated proapoptotic Bax. J Nutr. 2008; 138:1866–1871. [PubMed: 18806094]

37. Wu X, Zhang L, Gurley E, Studer E, Shang J, Wang T, Wang C, Yan M, Jiang Z, Hylemon PB, Sanyal AJ, Pandak WM, Zhou H. Prevention of free fatty acid–induced hepatic lipotoxicity by 18β-glycyrrhetinic acid through lysosomal and mitochondrial pathways. Hepatology. 2008; 47:1905–1915. [PubMed: 18452148]

38. Wanless IR, Shiota K. The pathogenesis of nonalcoholic steatohepatitis and other fatty liver diseases: a four-step model including the role of lipid release and hepatic venular obstruction in the progression to cirrhosis. Semin Liver Dis. 2004; 24:99–106. [PubMed: 15085490]

39. Saberi M, Bjelica D, Schenk S, Imamura T, Bandyopadhyay G, Li P, Vargeese C, Wang W, Bowman K, Zhang Y, Polisky B, Olefsky JM. Novel liver-specific TORC2 siRNA corrects hyperglycemia in rodent models of type 2 diabetes. Am J Physiol Endocrinol Metab. 2009

40. Park SY, Cho YR, Kim HJ, Hong EG, Higashimori T, Lee SJ, Goldberg IJ, Shulman GI, Najjar SM, Kim JK. Mechanism of glucose intolerance in mice with dominant negative mutation of CEACAM1. Am J Physiol Endocrinol Metab. 2006; 291:E517–524. [PubMed: 16638824]

41. Arkan MC, Hevener AL, Greten FR, Maeda S, Li ZW, Long JM, Wynshaw-Boris A, Poli G, Olefsky J, Karin M. IKK-beta links inflammation to obesity-induced insulin resistance. Nat Med. 2005; 11:191–198. [PubMed: 15685170]

42. Klein I, Cornejo JC, Polakos NK, John B, Wuensch SA, Topham DJ, Pierce RH, Crispe IN. Kupffer cell heterogeneity: functional properties of bone marrow derived and sessile hepatic macrophages. Blood. 2007; 110:4077–4085. [PubMed: 17690256]

43. Kennedy DW, Abkowitz JL. Kinetics of central nervous system microglial and macrophage engraftment: analysis using a transgenic bone marrow transplantation model. Blood. 1997; 90:986–993. [PubMed: 9242527]

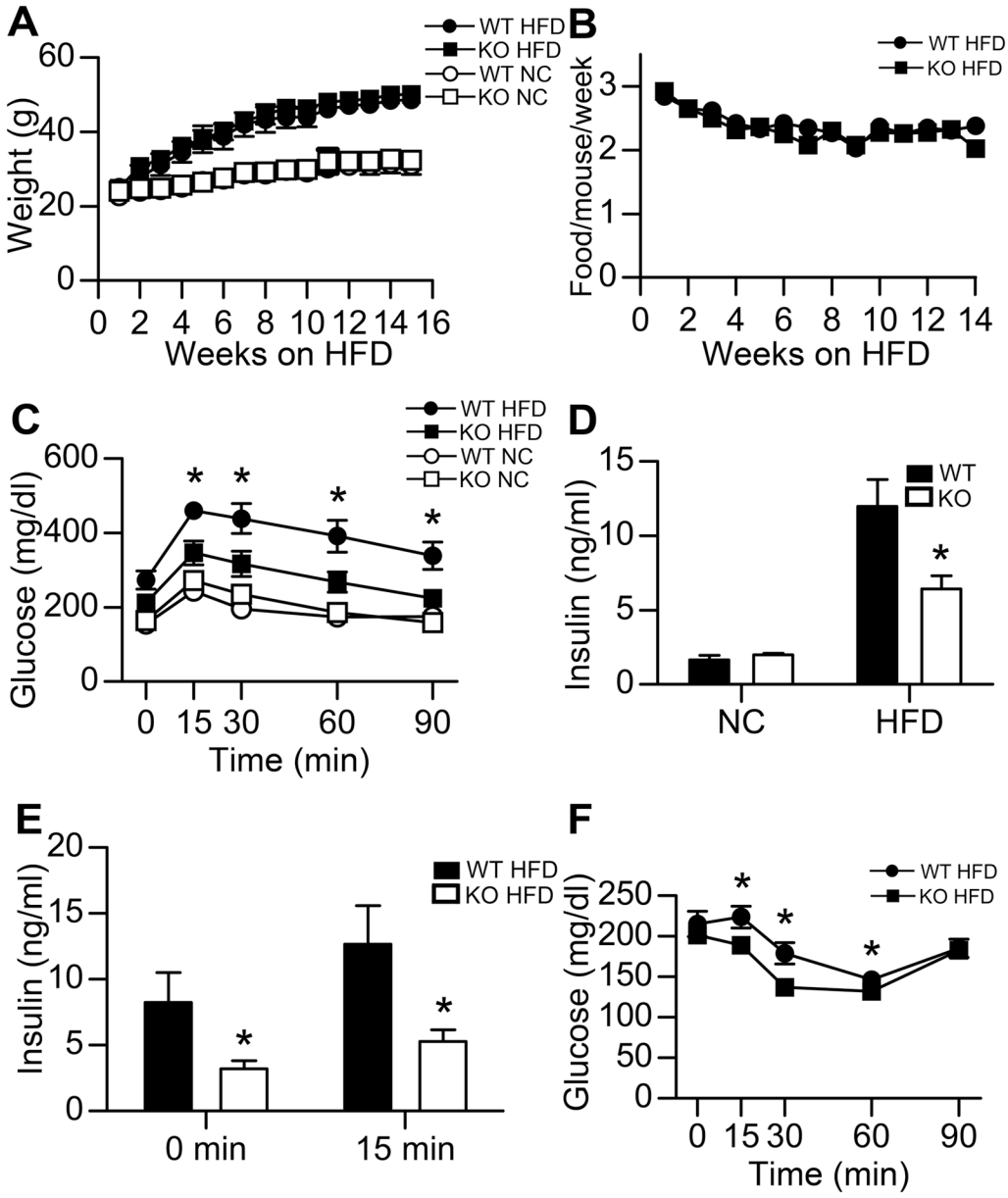


**Figure 1. Improved glucose homeostasis of GPR105 KO HFD-fed mice**

**(A)** Body weight gain of WT and GPR105 KO mice on NC and HFD (n=12 per group).

**(B)** Food intake of WT and GPR105 KO mice on HFD (n=12).

**(C)** Glucose tolerance testing in NC and HFD mice. Glucose (1 g/kg) was injected intraperitoneally after a 7h fast, and tail blood was collected for glucose measurement (n=8).

**(D)** Fasting insulin levels of WT and GPR105 KO mice on NC and HFD (n=8).

**(E)** Acute insulin secretion measured in HFD-fed WT and GPR105 KO mice at basal (7h fast) and 15 min after oral glucose challenge (n=8).

**(F)** Insulin tolerance testing in HFD mice. Intraperitoneal insulin (0.6 U/kg) was injected to 7h-fasted HFD WT and GPR105 KO mice. Blood glucose was measured at the indicated time points.

All values are expressed as means ± SEM. *$p < 0.05$ versus diet-matched WT.

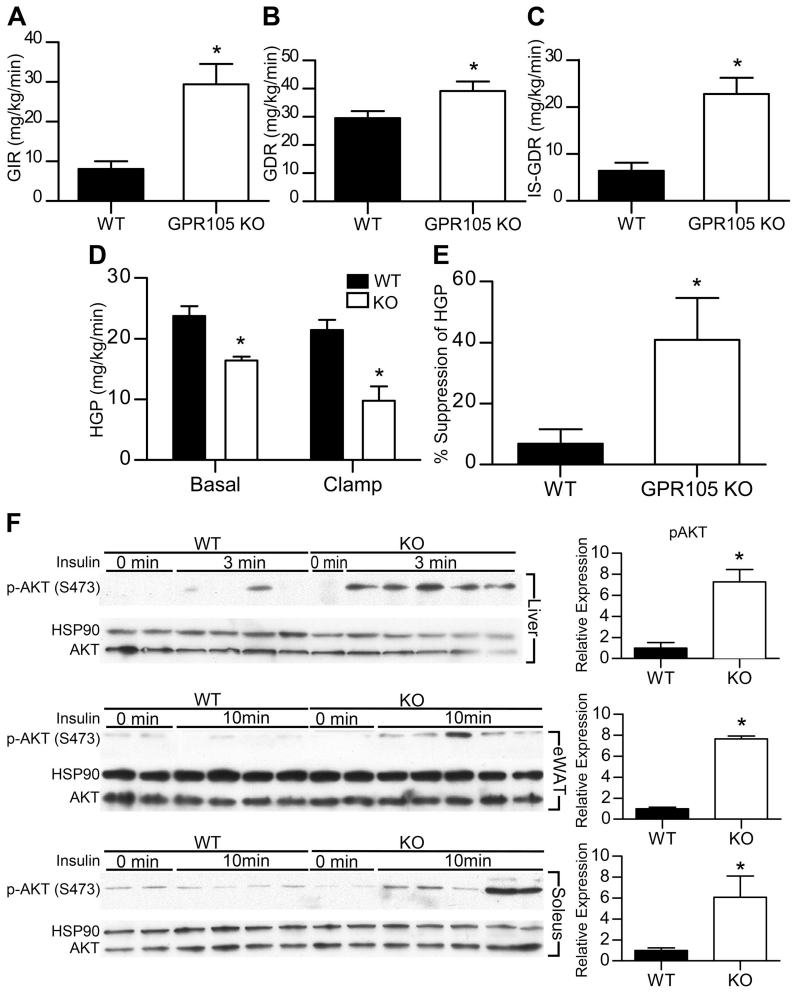


**Figure 2. Improved insulin sensitivity of GPR105 KO HFD-fed mice**

*In vivo* insulin sensitivity as determined by hyperinsulinemic-euglycemic clamp in WT (n=6) and GPR105 KO (n=6) mice fed HFD. GIR **(A)**, GDR **(B)**, IS-GDR **(C)**, basal and clamp HGP **(D)**, suppression of HGP **(E)**, are presented as means ± SEM. *$p < 0.05$ versus WT.

**(F)** Immunoblot analyses of Ser473 phosphorylation of Akt as well as total Akt and HSP90 in liver, adipose tissue and skeletal muscle. Tissues were collected before or at indicated time after insulin injection (0.2 U/kg) into the inferior vena cava.

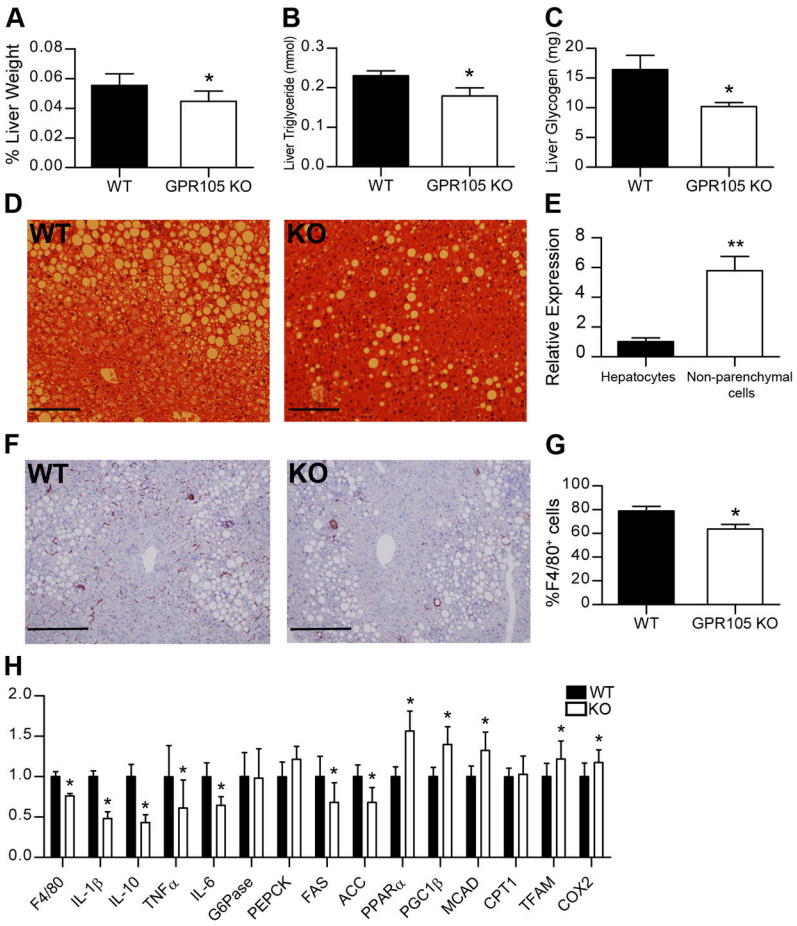


**Figure 3. Reduced macrophage infiltration and inflammation in liver**

Liver weight **(A)**, TG **(B)** and glycogen content **(C)** in liver are presented as means ± SEM. *$p < 0.05$ versus WT (n=6–12 per group).

**(D)** Representative images of H&E-stained liver sections of HFD-fed WT and GPR105 mice. Scale bars represent 50 μm.

**(E)** GPR105 expression in hepatocytes and non-parenchymal cells by quantitative PCR. Data are presented as means ± SEM. **p <0.005 (n=3). **(F)** Representative immunohistochemistry images of liver sections stained with anti-F4/80 antibody. Scale bars represent 50 μm.

**(G)** F4/80$^+$ cell as a percentage of all non-parenchymal cells by flow cytometry. *$p < 0.05$ versus WT (n=4).

**(H)** Gene expression in liver measured by quantitative PCR. Data are presented as means ± SD.

*$p < 0.05$ versus WT (n=8).

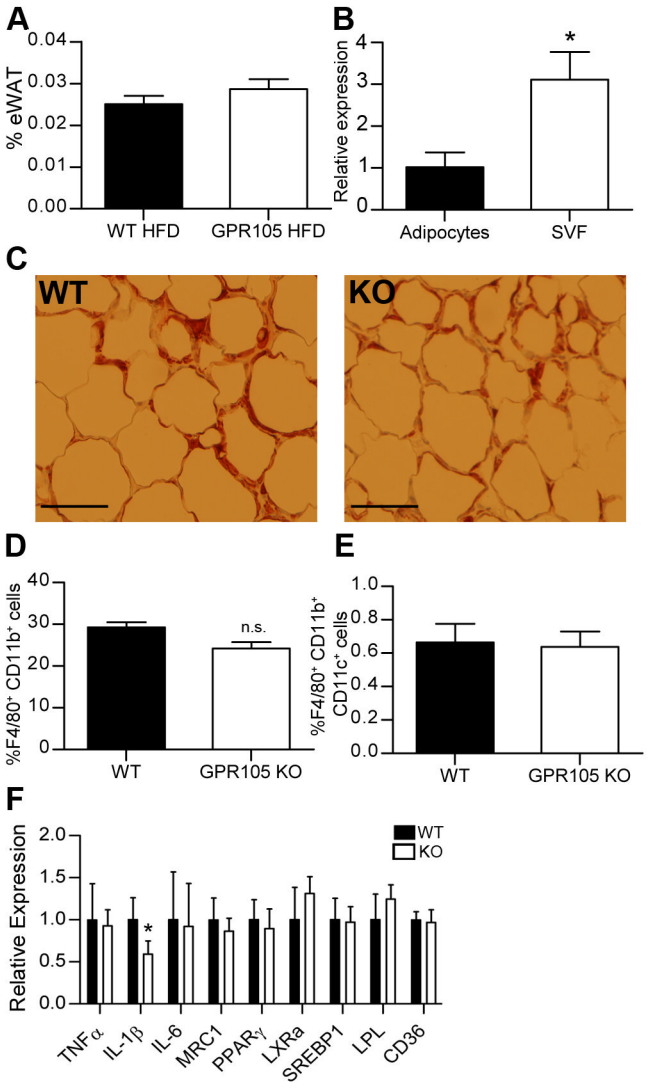


**Figure 4. Macrophages in adipose tissue**

**(A)** eWAT weight as a percentage of total body weight (n=8).

**(B)** GPR105 expression in adipocytes and SVF cells by quantitative PCR.

**(C)** Representative immunohistochemistry images of eWAT stained with anti-Mac2 antibody. Scale bars represent 100μm.

**(D)** F4/80$^+$CD11b$^+$ and **(E)** F4/80$^+$CD11b$^+$CD11c$^+$ cells in eWAT measured by flow cytometry (n=6).

**(F)** Gene expression in eWAT.

Data are presented as means ± SD. *$p < 0.05$ versus WT (n=8).

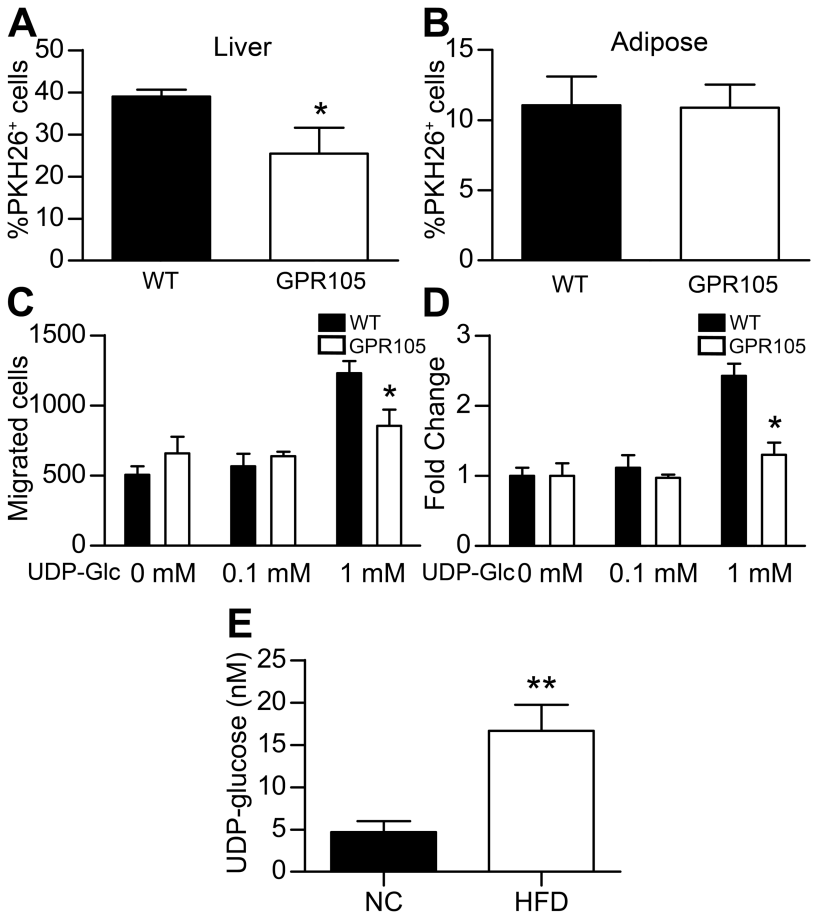


**Figure 5. GPR105-mediated chemotaxis *in vivo* and *in vitro***

PKH26$^+$ cells in liver non-parenchymal cells **(A)** and in eWAT SVF cells **(B)** of WT recipient mice 5 days after injection of labeled monocytes from WT or GPR105 KO donors (n=4). Data are presented as means ± SEM. *$p < 0.05$ versus WT.

**(C–D)** Chemotaxis of bone-marrow derived macrophages from WT or GPR105 KO mice towards a UDP-glucose gradient *in vitro* (data from 3 independent experiments). *$p < 0.05$ versus WT.

(E) Measurement of UDP-Glc in plasma from mice fed either normal chow (NC) or HFD (n = 8–10). **p <0.005.

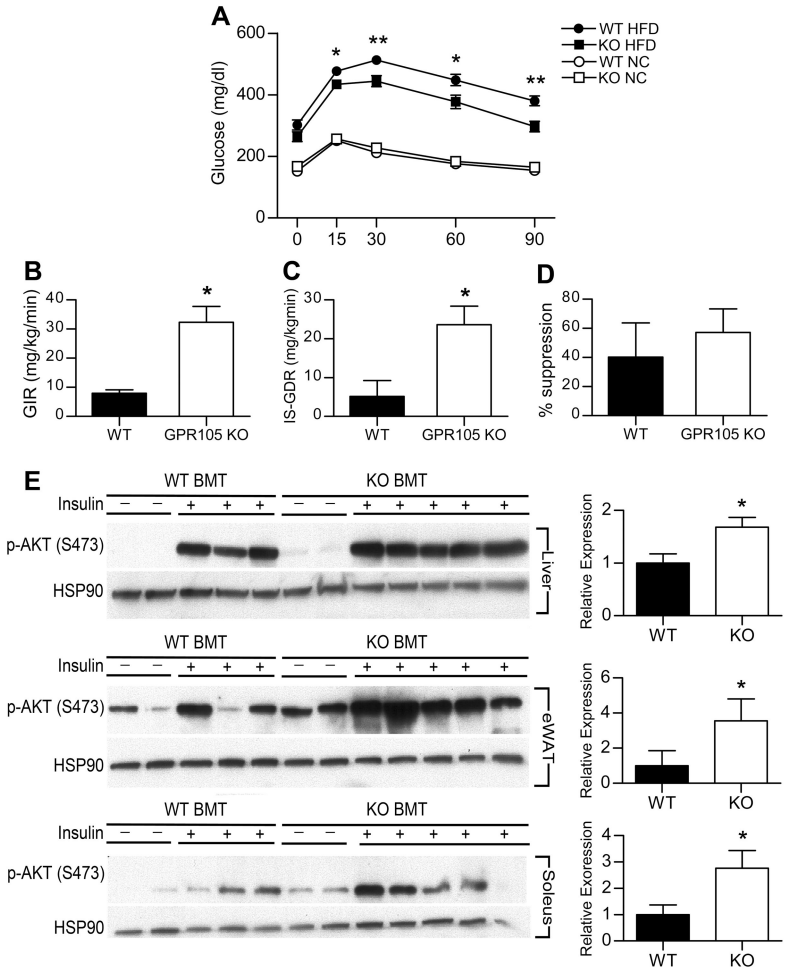


**Figure 6. Improved glucose homeostasis and insulin sensitivity of GPR105 KO bone marrow transplanted mice**

**(A)** Glucose tolerance testing in BMT-WT and BMT-KO mice on NC or HFD (n=12). *$p <$ 0.05 and **p < 0.005 versus diet-matched WT.

**(B–D)** Hyperinsulinemic-euglycemic clamp studies in BMT-WT (n=4) and BMT-KO (n=4) mice fed with HFD. GIR **(B)**, IS-GDR **(C)**, suppression of HGP **(D)**, are presented as means ± SEM. *$p < 0.05$ versus WT.

**(E)** Immunoblot analyses of Ser473 phosphorylation of Akt and HSP90 in liver, adipose tissue and skeletal muscles of BMT-WT and BMT-KO. Tissues were collected at the indicated times before and after insulin injection (0.2 U/kg). *$p < 0.05$ versus WT